Article

Multi-kingdom ecological drivers of microbiota assembly in preterm infants

https://doi.org/10.1038/s41586-021-03241-8

Received: 18 March 2020

Accepted: 14 January 2021

Published online: 24 February 2021

Check for updates

Chitong Rao[1,8], Katharine Z. Coyte[1,2,8]✉, Wayne Bainter[3], Raif S. Geha[3], Camilia R. Martin[4] & Seth Rakoff-Nahoum[1,5,6,7]✉

The gut microbiota of preterm infants develops predictably[1–7], with pioneer species colonizing the gut after birth, followed by an ordered succession of microorganisms. The gut microbiota is vital to the health of preterm infants[8,9], but the forces that shape these predictable dynamics of microbiome assembly are unknown. The environment, the host and interactions between microorganisms all potentially shape the dynamics of the microbiota, but in such a complex ecosystem, identifying the specific role of any individual factor is challenging[10–14]. Here we use multi-kingdom absolute abundance quantification, ecological modelling and experimental validation to address this challenge. We quantify the absolute dynamics of bacteria, fungi and archaea in a longitudinal cohort of 178 preterm infants. We uncover microbial blooms and extinctions, and show that there is an inverse correlation between bacterial and fungal loads in the infant gut. We infer computationally and demonstrate experimentally in vitro and in vivo that predictable assembly dynamics may be driven by directed, context-dependent interactions between specific microorganisms. Mirroring the dynamics of macroscopic ecosystems[15–17], a late-arriving member of the microbiome, *Klebsiella*, exploits the pioneer microorganism, *Staphylococcus*, to gain a foothold within the gut. Notably, we find that interactions between different kingdoms can influence assembly, with a single fungal species—*Candida albicans*—inhibiting multiple dominant genera of gut bacteria. Our work reveals the centrality of simple microbe–microbe interactions in shaping host-associated microbiota, which is critical both for our understanding of microbiota ecology and for targeted microbiota interventions.

Humans are colonized by vast communities of microorganisms, particularly within the gastrointestinal tract, that have key roles in the health of the host[8,9]. Infants are generally born uninhabited by microorganisms, and their gut microbiota gradually assembles after birth[1–7]. Notably, this developmental process occurs in a predictable manner, with specific bacterial taxa establishing in the gut at distinct points in infant life[18–22]. The early-life microbiota is critical to infant health, and microbiota composition is linked to a range of diseases, morbidity and mortality, particularly within preterm infants[1,23–27]. Yet despite its importance, we do not understand what drives the patterned progressions of the infant gut community[11–13]. Gestational age, delivery mode, host epithelial and immune ontogeny, diet, antibiotics and the interactions between individual microorganisms may each influence microbiota composition[2,7,18–22,28,29]. But with such complexity, the effect of any individual factor on the development of the microbiota has remained unclear, and disentangling how and why microbial communities change over time remains a major challenge—both for the human microbiota and for host-associated and environmental microbiomes more broadly.

Our ability to identify drivers of microbiota development has been hampered by the complexity of microbial ecosystems and also by fundamental limitations in how we quantify the composition of microbial communities[10–13]. First, although next-generation sequencing (NGS) has provided a comprehensive map of bacterial diversity within the human gut[30,31], we still know little about the other microorganisms—such as fungi and archaea—that colonize the infant microbiota[32–34], which constrains our ability to identify inter-kingdom interactions that drive ecosystem dynamics[35]. Second, NGS data typically chart only the relative abundances of taxa, providing the proportions of different microorganisms within a community, but not the absolute amounts. If a species increases in relative abundance over time we cannot determine whether that species is blooming or others are dying out (Fig. 1a). The compositional nature of relative abundance data can thus mask community dynamics, which undermines our ability to identify biotic and abiotic forces that shape changes in the microbiota[36–38]. Here we used a scalable multi-kingdom quantification method to map absolute microbiota dynamics in a longitudinal cohort of preterm infants. Combining ecological models with in vitro and in vivo validation, we

[1]Division of Infectious Diseases, Department of Pediatrics, Boston Children's Hospital, Boston, MA, USA. [2]Division of Evolution and Genomic Sciences, School of Biological Sciences, University of Manchester, Manchester, UK. [3]Division of Immunology, Department of Pediatrics, Boston Children's Hospital, Boston, MA, USA. [4]Department of Neonatology and Division of Translational Research, Beth Israel Deaconess Medical Center, Boston, MA, USA. [5]Division of Gastroenterology, Department of Pediatrics, Boston Children's Hospital, Boston, MA, USA. [6]Department of Microbiology, Harvard Medical School, Boston, MA, USA. [7]Broad Institute of MIT and Harvard, Cambridge, MA, USA. [8]These authors contributed equally: Chitong Rao, Katharine Z. Coyte. ✉e-mail: katharine.coyte@manchester.ac.uk; seth.rakoff-nahoum@childrens.harvard.edu

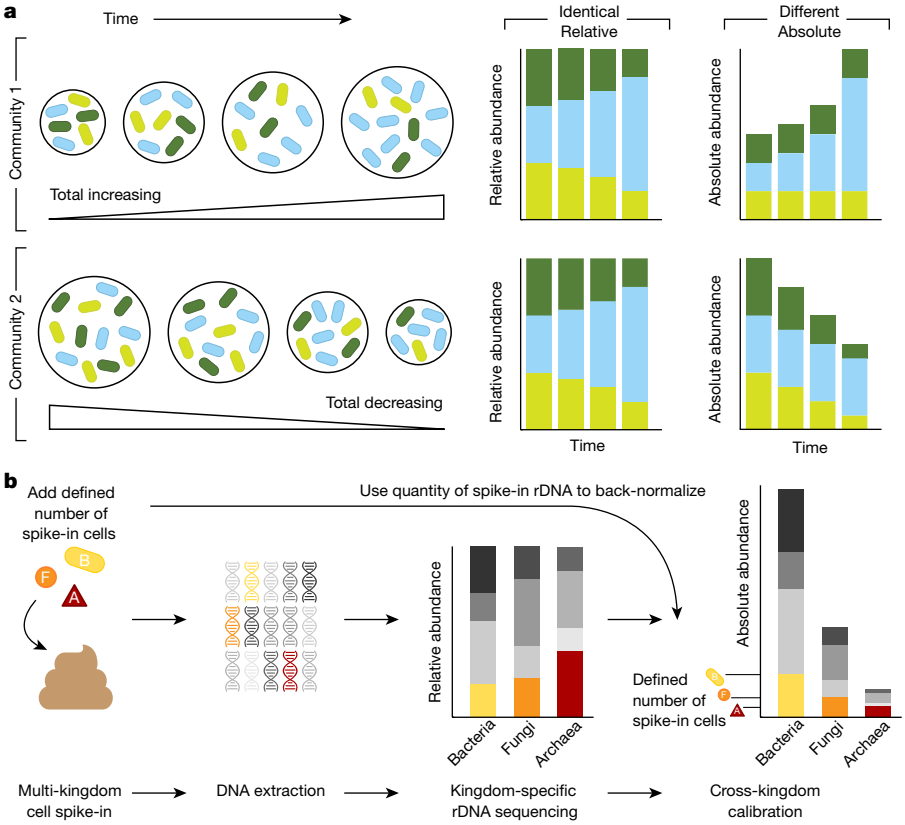

Fig. 1 | MK-SpikeSeq enables robust quantification of absolute abundances. a, Schematic illustrating how relative abundance data can mask underlying community dynamics, rendering it challenging to distinguish different ecological scenarios. **b**, Overview of the MK-SpikeSeq pipeline. Before DNA extraction, defined amounts of each spike-in cell (bacteria (B), fungi (F) and archaea (A)) are added to each microbiome sample. Relative abundances of each microbial kingdom are then quantified using standard kingdom-specific rDNA amplicon sequencing. As the absolute abundances of rDNA for each spike-in cell are known, these quantities can be used as back-normalization factors to calculate the absolute abundances of all other organisms present in each sample. The spike-in cells also serve as internal controls for the entire sample-processing procedure, rendering the absolute quantification robust to factors such as sample-to-sample variability in DNA extraction efficiency.

reveal that within- and between-kingdom microbial interactions shape the predictability of early-life microbiome assembly.

Quantifying multi-kingdom abundances

To identify drivers of change within any microbial community, it is necessary to quantify the absolute changes in community members over time. To achieve this, we developed a cell-based multi-kingdom spike-in method (MK-SpikeSeq) that quantifies the absolute abundances of bacteria, fungi and archaea simultaneously within any given microbiome (Fig. 1b, Supplementary Information). Specifically, we add to each sample defined numbers of exogenous microbial cells of each kingdom and perform kingdom-specific ribosomal DNA (rDNA) amplicon sequencing to obtain relative abundances in each kingdom. The spike-in cells serve as internal controls for sample processing and, as spike-in cell abundances are known, we can then back-normalize and calculate absolute abundances of all community members (Fig. 1b, Supplementary Fig. 1). As our primary objective was to study mammalian microbiota, our spike-in contained the bacterium *Salinibacter ruber*[39], the fungus *Trichoderma reesei* and the archaeon *Haloarcula hispanica*, selected on the basis of their absence or rarity in mammalian microbiomes (Supplementary Table 2). However, our approach can be adapted by choosing the spike-in to target any host-associated or environmental microbiome, and can be combined with shotgun metagenomics to capture viruses and enable strain-level quantification. We validated the ability of MK-SpikeSeq to measure absolute abundances using a series of defined mock communities, and then compared the performance of MK-SpikeSeq to that of existing approaches for absolute abundance quantification (total DNA, cytometry-based imaging, quantitative PCR (qPCR) and DNA-based spike-in) using a set of test samples (Supplementary Information, Extended Data Figs. 1–5). Together, these data showed that MK-SpikeSeq generates highly sensitive and robust measurements of absolute abundances for individual taxa across multiple kingdoms—a key requisite for identifying drivers of microbiota dynamics.

Multi-kingdom microbiota assembly dynamics

Having validated MK-SpikeSeq, we built a high-resolution multi-kingdom picture of infant microbiota dynamics. We assembled a prospective cohort of 178 preterm infants from a tertiary-care neonatal intensive care unit (NICU). The assembly of the preterm microbiota differs substantially from that of term infants. Most preterm infants are born by Caesarean section and thus are seeded with skin- and hospital-associated microorganisms, and are devoid of key maternally derived bacteria[7,21,29]. The preterm microbiota also exhibits 'delayed' maturity, with a prolonged membership of facultative anaerobic bacteria compared to the predominantly strict anaerobic community of term infants[7,21,29]. We focused on preterm infants owing to their clinical relevance and because they are amenable to high-frequency longitudinal sampling with readily available clinical metadata. These features render the preterm gut an important and tractable system for establishing a proof-of-principle understanding of the assembly of the microbiota. We sampled each infant within our cohort on approximately their 1st, 14th, 28th and 42nd day of life, and for 13 infants we gathered nearly daily stools for their first 6 weeks of life (940 samples in total). Together, this cohort enabled us to build a high-resolution picture of microbiota development within the preterm infant gut.

Consistent with previous studies[18–23], we observed that bacterial communities in the preterm infant gut cluster primarily into four distinct community states that are characterized by the domination of one of four genera: *Staphylococcus*, *Klebsiella*, *Escherichia* or *Enterococcus* (Fig. 2a). In contrast to full-term infants, these microbiome clusters were independent of diet or delivery mode (Extended Data Fig. 6). Notably, the bacterial community within our preterm cohort, as previously observed[18–23], developed in a predictable and highly dynamic manner over time. Most infants were dominated by *Staphylococcus* at first, and then transitioned to a state dominated by *Klebsiella*, *Enterococcus* or *Escherichia* as they aged (Fig. 2a, b, Extended Data Fig. 6), with the total bacterial load in the infant gut gradually increasing over time (Fig. 2f, g, Extended Data Fig. 7). Comparing the absolute and relative abundances of these dominant genera illustrated how

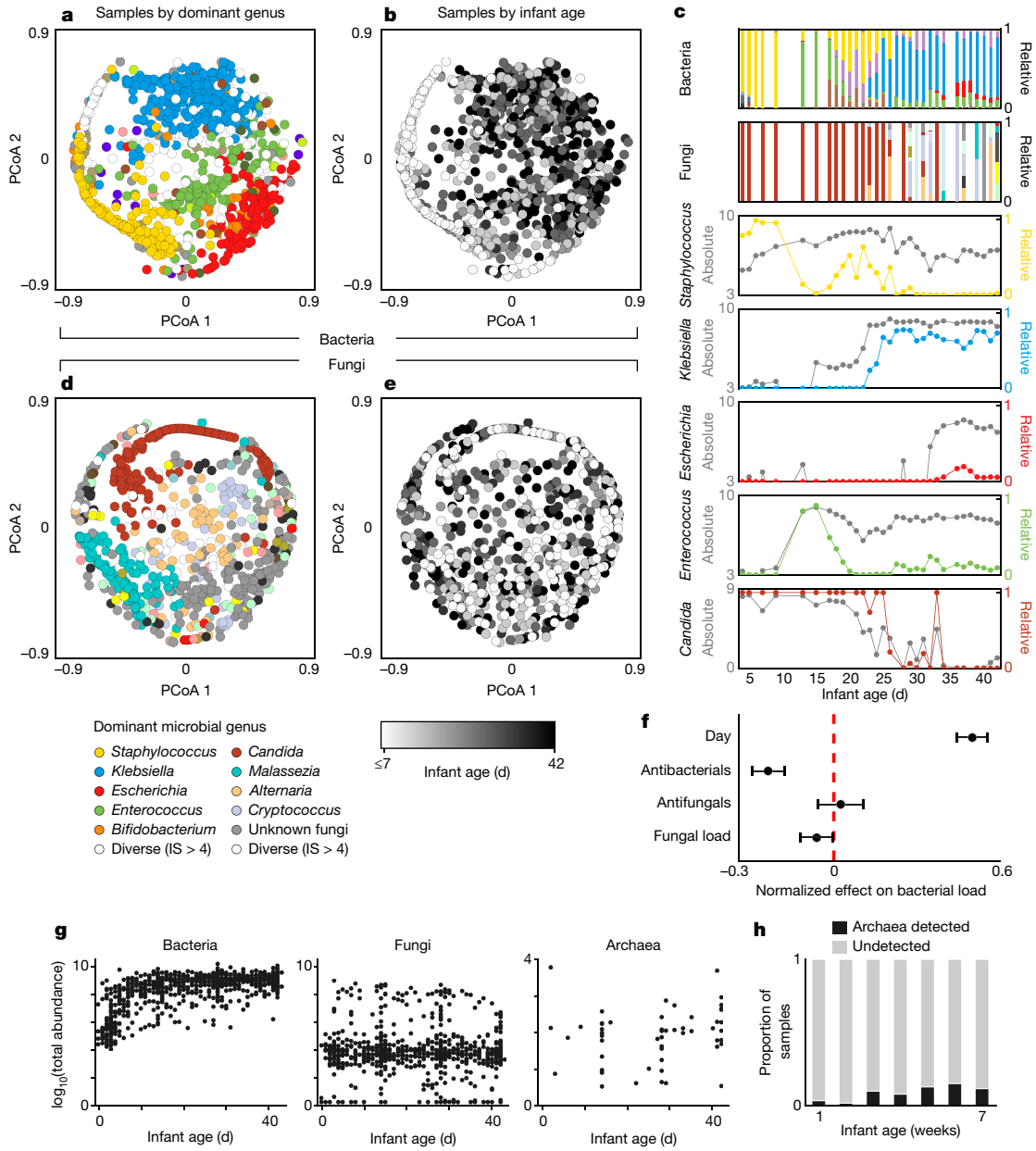

Fig. 2 | The gut of preterm infants exhibits rich bacterial and fungal community dynamics. a, Principal coordinate analysis (PCoA) plot of Bray–Curtis dissimilarities between bacterial samples at the genus level. Each dot represents a sample, coloured by the dominant genus present or white if diversity was high (inverse Simpson index (IS) > 4). **b**, The same PCoA as **a** with samples instead coloured by infant day of life, illustrating how bacterial community composition changes predictably over time. **c**, Microbiota dynamics of a single representative infant, highlighting the importance of gathering absolute abundances when studying microbiome ecology. Stacked bars represent total community composition (for full colour schemes, see Extended Data Figs. 3, 4). Line plots illustrate the relative (coloured) and absolute (grey) abundances of individual genera. **d**, **e**, PCoA plots of fungal community composition coloured by dominant genus (**d**) or infant age (**e**), indicating that fungal community composition does not correlate with infant age. **f**, Effects of clinical and microbial factors on total bacterial load, quantified by a linear mixed-effects model, suggesting a potential relationship between kingdoms within the preterm infant gut (centres and error bars indicate estimated fixed effects and 95% confidence intervals, respectively). **g**, Total abundances of bacteria, fungi and archaea over time. **h**, Proportion of samples in which archaea could be detected during each week of life. For **a**, **b**, **g** (left), number of samples (n) = 934; for **d**, **e**, **g** (centre), n = 772; for **f**, n = 770; for **g** (right), **h**, n = 596.

compositional data can misattribute both how and when communities change. In several infants, relative abundances initially masked blooms in *Klebsiella* and *Escherichia*, and showed *Staphylococcus* and *Enterococcus* collapsing in the community when their abundances were instead comparatively stable (Fig. 2c, Supplementary Figs. 2–16). Such comparisons also indicated that, although the bacterial communities within our cohort were typically dominated by just one genus, often the other major genera remained stable at high levels within the preterm infant gut (Supplementary Figs. 2–16).

In contrast to the predictable dynamics of bacterial communities, we uncovered diverse but unpredictable fungal communities within the preterm infant gut. On average, fungal dynamics were noisier and exhibited less temporal structure than bacterial communities, with no clear correlation between fungal community composition or load and infant age (Fig. 2d, e, Extended Data Fig. 8). Notably, although rarely occurring in adults[32], *Cryptococcus* was the dominant fungal genus in approximately 5% of samples; whereas *Saccharomyces* species[32] were detected in only five infants, despite being a common inhabitant of the

adult gut. As with bacterial communities, MK-SpikeSeq uncovered fungal blooms and collapses masked by relative abundances. For example, in several infants *Candida* stably maintained a high relative abundance, despite dropping multiple orders of magnitude in absolute load over time (Fig. 2c, Supplementary Figs. 4–18). However, although the fungal dynamics were themselves unpredictable, a linear mixed-effects model that accounted for infant age, antibacterial agents and antifungal agents revealed a weak negative correlation between bacterial and fungal loads (normalized effect size, −0.060; 95% Wald confidence interval, [−0.119, −0.001]) (Fig. 2f, Extended Data Fig. 7). That is, when accounting for clinical covariates, samples with higher fungal loads tended to have lower bacterial loads. This inverse relationship led us to wonder whether cross-kingdom interactions might be influencing preterm microbiota dynamics.

Archaea were rare within our cohort, with most samples showing no archaeal signal. However, we detected a weak positive trend in both the frequency of archaeal detection (X^2 test for trend, $P = 0.002$) and total archaeal load over time (Spearman's $R = 0.13$, $P = 0.002$), with higher archaeal abundances generally detected in later weeks of life (Fig. 2g, h, Extended Data Fig. 7).

Ecological drivers of microbiota assembly

Having generated a high-resolution multi-kingdom map of the assembly of the microbiota in infants, we next sought to identify factors that drive the predictable dynamics observed. To achieve this, we used Bayesian regularized regression to fit our longitudinal data to an extended generalized Lotka–Volterra (gLV) model, an approach only possible with absolute abundances. The gLV model assumes that the growth rate of an individual taxon depends on the taxon's intrinsic growth rate and interaction with kin, the effect of clinically administered antimicrobials and interactions between the focal taxon and other community members[40–42] (Fig. 3a, Supplementary Information). Specifically, the model allows microorganisms to interact in a number of different ways—from bidirectional competition (−/−) such as nutrient competition, to exploitation (+/−), in which one microorganism takes advantage of another—or to not interact at all (0/0). The model also allows each clinically administered antimicrobial agent to inhibit, promote or have no effect on each microorganism. Together this yields a highly parameterized model of community dynamics, which we fitted to our data using a conservative regularization framework. By doing so, we were able to identify those microbe–microbe or antibiotic–microbe interactions that have a strong, consistent role in shaping community dynamics, while avoiding overfitting and filtering weak interactions that do not influence community dynamics. This approach thus enabled us to disentangle the effects of different biotic and abiotic interactions on microbiota assembly, independently of missing community members (for example, viruses), or underlying host variability.

Our ecological inference predicted that strong intra- and inter-kingdom interactions between specific microbial genera have a pivotal role in shaping the assembly of the microbiota in the infant gut (Fig. 3b, Extended Data Fig. 9, Supplementary Information). Of note, we inferred that the early colonizing *Staphylococcus* enhanced growth of *Klebsiella* within the infant gut but was itself inhibited by *Klebsiella*. Thus our model suggests that the characteristic transition observed in preterm infants from the domination of *Staphylococcus* to that of *Klebsiella* (Fig. 2a, b) is shaped, in part, by *Klebsiella* exploiting the early colonizer. We also inferred that *Klebsiella* itself was inhibited by another dominant genus, *Enterococcus*, suggesting that the distinct domination states of these two genera may be partly driven by one excluding the other. Most notably, consistent with the inverse correlation between bacterial and fungal loads, our analyses suggested that between-kingdom interactions have a key role in community dynamics. Specifically, we inferred that the fungal genus *Candida* inhibited both *Klebsiella* and *Escherichia*, but was itself inhibited by *Staphylococcus*. These results suggested not only that diverse fungal communities are present in preterm infants, but that members of these communities influence overall community dynamics.

Notably, we discovered that a substantial proportion of the interactions that shape the microbiota assembly of preterm infants are exploitative (+/−), with these asymmetric interactions comprising over 20% of inferred microbe–microbe interactions (Extended Data Fig. 9c). The importance of these directed, asymmetric interactions in shaping the assembly of the microbiota underlines the power of our absolute-abundance-based approach. Without absolute abundances, ecological inferences are limited to correlational analyses. These analyses identify positive or negative correlations between taxa, but cannot determine directionally which taxa are interacting with which, nor identify asymmetric interactions[36,43–45]. As a consequence, correlational analyses cannot identify exploitative, commensal or amensal interactions. Indeed, when applied to our dataset, correlational analyses of relative abundance[46] erroneously inferred that *Staphylococcus* inhibited *Klebsiella* and promoted *Candida* (Extended Data Fig. 9d). In other words, relative abundances and correlation analysis not only misrepresented the dynamics of infant microbiome assembly (Fig. 2), but also misclassified the ecological processes that underlie these dynamics.

Validation of interactions shaping assembly

Our ecological inference indicated that microbe–microbe interactions are central to predictable assembly of the gut microbiome in infants. However, although we used a conservative regularization framework to ensure robustness to spurious correlations, our predictions may still be vulnerable to unobserved confounding factors that are not incorporated in the model, such as diet, viruses or the host. Indeed, although a number of studies have used similar modelling approaches to infer interactions, few predictions have been experimentally validated[42,47,48]. We therefore sought to determine whether we could reproduce our inferred interactions in a reductionist experimental system. Focusing first on our predicted within-kingdom interactions, we isolated *Staphylococcus*, *Klebsiella*, *Escherichia* and *Enterococcus* strains from five infants in our cohort, capturing several distinct species of each genus (Supplementary Table 13). We then performed monoculture and pairwise co-culture of these strains and used colony-forming units (CFU) to determine the pairwise fitness effects of strains on one another (Supplementary Table 14). We were able to reproduce in vitro all of the inhibitory interactions predicted by our model, with growth effects largely conserved within genera (Fig. 3c). *Klebsiella* strongly inhibited *Staphylococcus*, reducing *Staphylococcus* yields by over 1,000-fold, whereas *Enterococcus* variably but consistently inhibited *Klebsiella* (Fig. 3c). As predicted, *Klebsiella* showed no effect on *Enterococcus*, consistent with this interaction being amensalism rather than bidirectional competition, and thus validating the directionality of our inference.

In contrast to our prediction that *Staphylococcus* benefitted *Klebsiella* during microbiome assembly, we did not observe a positive effect of *Staphylococcus* on *Klebsiella* in vitro (Fig. 3c). Given the strength of the predicted *Klebsiella*–*Staphylococcus* exploitation, we hypothesized that this interaction may be context-dependent. That is, we hypothesized that, owing to differing environments in vitro versus in vivo, *Klebsiella* might only benefit from *Staphylococcus* within the gut. To investigate this, we used two co-resident NICU isolates—*Klebsiella pneumoniae* and *Staphylococcus epidermidis*—to test whether *Klebsiella* benefited from *Staphylococcus* in vivo in the mammalian gut, using a mouse model of intestinal colonization (Fig. 3d). We used CFU counts and MK-SpikeSeq to measure the fitness of *K. pneumoniae* in mice pre-colonized with or without *S. epidermidis* (Fig. 3d, Extended Data Fig. 10a, c). As predicted, *S. epidermidis* significantly enhanced the ability of *K. pneumoniae* to colonize the mouse gut, with

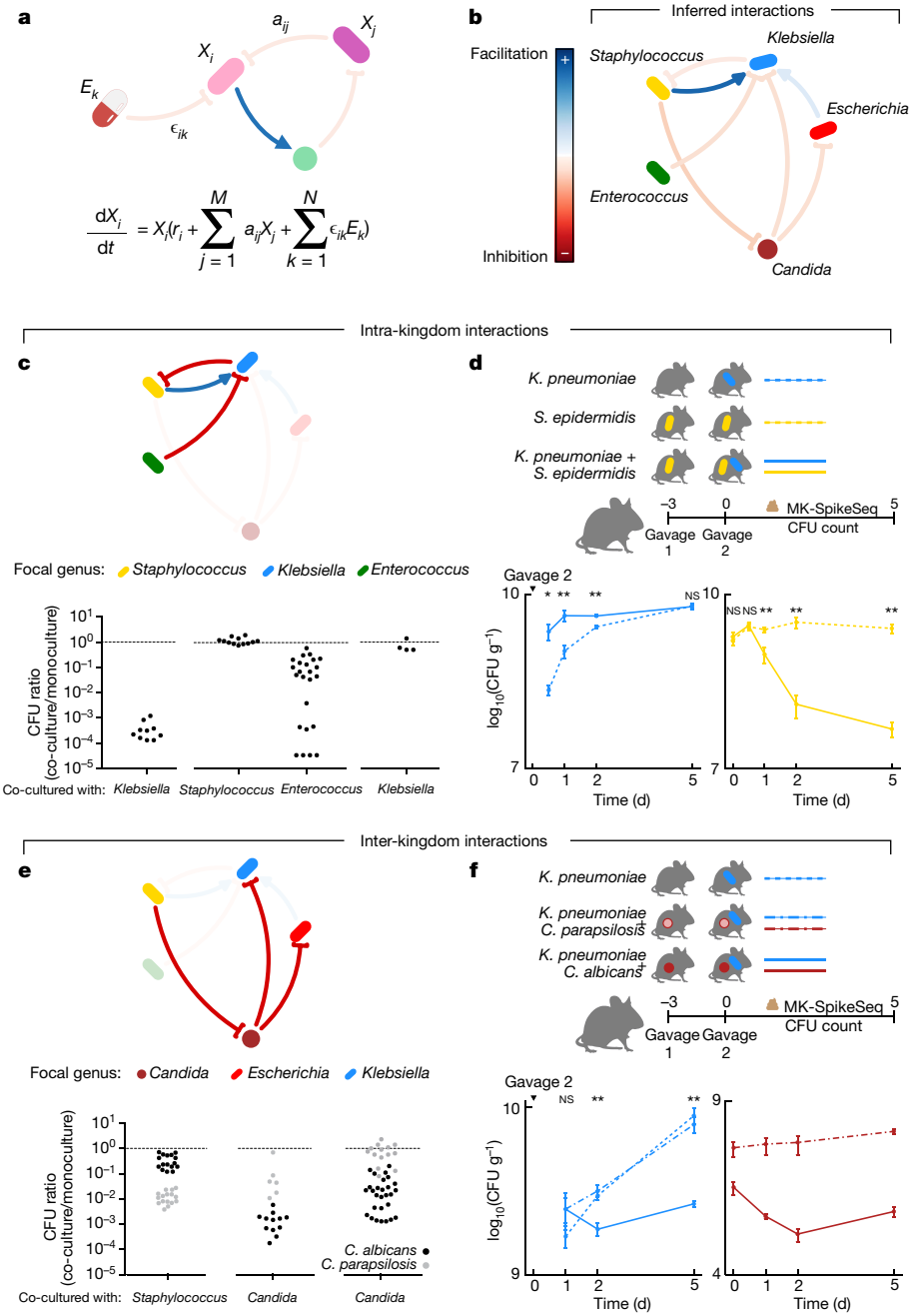

Fig. 3 | Pairwise intra- and inter-kingdom interactions drive predictable patterns of microbiome assembly in the infant gut. a, Schematic illustrating the gLV model used to identify causative drivers of bacterial and fungal dynamics within the infant gut. This model assumes the growth rate of each taxon, dX_i/dt, is determined by its own intrinsic growth rate r_i, its interaction with other community members $a_{ij}X_j$, and any environmental perturbation $\epsilon_{ik}E_k$. **b**, The gLV model identified a network of microbe–microbe interactions occurring between dominant members of the microbiota of the preterm infant gut that are predicted to affect microbiota dynamics. **c**, In vitro growth effects of isolates from infants on one another using monoculture and pairwise co-culture, testing the predicted within-kingdom interactions. **d**, CFU counts quantifying microbial fitness in vivo in a specific-pathogen-free (SPF) mouse model, reproducing the predicted exploitation of *Staphylococcus* by *Klebsiella*. Gavage 2 indicates the day of inoculation with *K. pneumoniae*. **e**, In vitro growth of isolates from infants in monoculture and pairwise co-culture, testing the predicted cross-kingdom interactions. Black and grey dots indicate co-cultures with *C. albicans* and *C. parapsilosis*, respectively. **f**, CFU counts quantifying microbial fitness in vivo in a SPF mouse model, reproducing the species-specific differences in the cross-kingdom inhibition observed in vitro. Gavage 2 indicates the day of inoculation with *K. pneumoniae*. For **c**, **e**, each dot denotes one unique pair of strains of the indicated genera, with each pair replicated at least once (Supplementary Table 14a). For **d**, **f**, *Klebsiella* was undetected at time 0 at gavage; $n = 5$ per group; data are mean ± s.e.m.; $^*P < 0.05$, $^{**}P < 0.01$, NS, not significant (by two-tailed Student's *t*-test); see Supplementary Table 15 for exact *P* values; see Extended Data Fig. 10c, d for repeats of in vivo experiments.

K. pneumoniae exhibiting faster colonization if the gut was pre-colonized with *S. epidermidis* (Fig. 3d). Moreover, mice that were colonized with *K. pneumoniae* had significantly reduced levels of *S. epidermidis* compared to those colonized without *K. pneumoniae*, with *S. epidermidis* declining alongside the increase in levels of *K. pneumoniae* (Fig. 3d). These in vivo data recapitulated the dynamics observed in the microbiome assembly of infants (Fig. 2c) and suggested that the predictable patterns in the assembly of infants may indeed be due to exploitation of an early pioneer by a late colonizer. These data also underlined the importance of context when studying microbiota interactions, illustrating how taxa may interact differently in vitro versus within a host.

Having validated our inferred within-kingdom interactions, we sought to validate the between-kingdom interactions predicted to influence the gut assembly of preterm infants (Fig. 3e). Again using isolates from infants, each of our predicted between-kingdom interactions could also be reproduced within our in vitro system (Fig. 3e). As predicted, *Candida* members caused an approximately 100–1,000-fold inhibition of each Enterobacteriaceae isolate and experienced a growth reduction of around 10–100-fold when co-cultured with *Staphylococcus*, consistent with previous observations[49]. Notably, we observed a bimodal distribution in the strength of inhibition of different *Candida* isolates by *Staphylococcus* (Fig. 3e), with the two modes corresponding to two *Candida* species—*Candida albicans* and *Candida parapsilosis*. Moreover, these two species also exerted differing inhibitory effects on Enterobacteriaceae; overall, *C. albicans* both resisted *Staphylococcus* and inhibited Enterobacteriaceae more than *C. parapsilosis* did (Fig. 3e). To examine whether this species-specific inhibition of Enterobacteriaceae by *Candida* occurred in vivo, we pre-colonized mice with *C. albicans*, *C. parapsilosis* or vehicle control, then introduced *K. pneumoniae* and measured microbial colonization dynamics. We observed a significantly reduced colonization of *K. pneumoniae* in mice that were pre-colonized with *C. albicans*, compared to control mice or those that were pre-colonized with *C. parapsilosis*, validating both

the species specificity in the fungi–bacteria interaction and its occurrence within the mammalian gut (Fig. 3f, Extended Data Fig. 10b, d). Together, our data reveal a species-specific cross-kingdom interaction that appears to shape the microbiota of preterm infants.

Discussion

The de novo assembly of the infant gut microbiome is notably ordered, with pioneer microorganisms colonizing first, followed by predictable waves of other microorganisms. However, the forces that drive these predictable transitions have so far remained unknown. Priority effects, diet, antibiotics and the developing immune system are all thought to affect microbiota dynamics, but given that there are multiple interacting factors at play, disentangling the role of any individual process has proved difficult. Here we show that a combination of multi-kingdom absolute abundance quantification, ecological modelling and experimental validation can be used to overcome this challenge. We have demonstrated that the predictable patterns of assembly of the preterm infant gut microbiota can be driven by direct, context-dependent interactions between microorganisms. Our findings suggest a common mechanism of assembly between the infant microbiota and macroscopic ecological succession. Just as in macroscopic ecosystems[15–17], microorganisms may exploit one another to establish within the infant gut, and direct interactions between kingdoms appear to have a central role in community dynamics. The reducibility of gut microbiota assembly to simple, pair-wise interactions has profound implications for understanding and ultimately manipulating microbial ecosystems in health and disease.

Online content

Any methods, additional references, Nature Research reporting summaries, source data, extended data, supplementary information, acknowledgements, peer review information; details of author contributions and competing interests; and statements of data and code availability are available at https://doi.org/10.1038/s41586-021-03241-8.

1. Charbonneau, M. R. et al. A microbial perspective of human developmental biology. *Nature* **535**, 48–55 (2016).
2. Bäckhed, F. et al. Dynamics and stabilization of the human gut microbiome during the first year of life. *Cell Host Microbe* **17**, 690–703 (2015).
3. Stewart, C. J. et al. Temporal development of the gut microbiome in early childhood from the TEDDY study. *Nature* **562**, 583–588 (2018).
4. Derrien, M., Alvarez, A. S. & de Vos, W. M. The gut microbiota in the first decade of life. *Trends Microbiol.* **27**, 997–1010 (2019).
5. Yatsunenko, T. et al. Human gut microbiome viewed across age and geography. *Nature* **486**, 222–227 (2012).
6. Lim, E. S. et al. Early life dynamics of the human gut virome and bacterial microbiome in infants. *Nat. Med.* **21**, 1228–1234 (2015).
7. Palmer, C., Bik, E. M., DiGiulio, D. B., Relman, D. A. & Brown, P. O. Development of the human infant intestinal microbiota. *PLoS Biol.* **5**, e177 (2007).
8. Lynch, S. V. & Pedersen, O. The human intestinal microbiome in health and disease. *N. Engl. J. Med.* **375**, 2369–2379 (2016).
9. Honda, K. & Littman, D. R. The microbiota in adaptive immune homeostasis and disease. *Nature* **535**, 75–84 (2016).
10. Fischbach, M. A. Microbiome: focus on causation and mechanism. *Cell* **174**, 785–790 (2018).
11. Widder, S. et al. Challenges in microbial ecology: building predictive understanding of community function and dynamics. *ISME J.* **10**, 2557–2568 (2016).
12. Vrancken, G., Gregory, A. C., Huys, G. R. B., Faust, K. & Raes, J. Synthetic ecology of the human gut microbiota. *Nat. Rev. Microbiol.* **17**, 754–763 (2019).
13. Walter, J., Armet, A. M., Finlay, B. B. & Shanahan, F. Establishing or exaggerating causality for the gut microbiome: lessons from human microbiota-associated rodents. *Cell* **180**, 221–232 (2020).
14. Wolfe, B. E., Button, J. E., Santarelli, M. & Dutton, R. J. Cheese rind communities provide tractable systems for in situ and in vitro studies of microbial diversity. *Cell* **158**, 422–433 (2014).
15. Connell, J. H. & Slatyer, R. O. Mechanisms of succession in natural communities and their role in community stability and organization. *Am. Nat.* **111**, 1119–1144 (1977).
16. Bertness, M. D. & Callaway, R. Positive interactions in communities. *Trends Ecol. Evol.* **9**, 191–193 (1994).
17. Shade, A. et al. Macroecology to unite all life, large and small. *Trends Ecol. Evol.* **33**, 731–744 (2018).
18. Gregory, K. E. et al. Influence of maternal breast milk ingestion on acquisition of the intestinal microbiome in preterm infants. *Microbiome* **4**, 68 (2016).
19. Gibson, M. K. et al. Developmental dynamics of the preterm infant gut microbiota and antibiotic resistome. *Nat. Microbiol.* **1**, 16024 (2016).
20. DiBartolomeo, M. E. & Claud, E. C. The developing microbiome of the preterm infant. *Clin. Ther.* **38**, 733–739 (2016).
21. La Rosa, P. S. et al. Patterned progression of bacterial populations in the premature infant gut. *Proc. Natl Acad. Sci. USA* **111**, 12522–12527 (2014).
22. Costello, E. K., Carlisle, E. M., Bik, E. M., Morowitz, M. J. & Relman, D. A. Microbiome assembly across multiple body sites in low-birthweight infants. *MBio* **4**, e00782-13 (2013).
23. Stewart, C. J. et al. Temporal bacterial and metabolic development of the preterm gut reveals specific signatures in health and disease. *Microbiome* **4**, 67 (2016).
24. Pammi, M. et al. Intestinal dysbiosis in preterm infants preceding necrotizing enterocolitis: a systematic review and meta-analysis. *Microbiome* **5**, 31 (2017).
25. Gasparrini, A. J. et al. Persistent metagenomic signatures of early-life hospitalization and antibiotic treatment in the infant gut microbiota and resistome. *Nat. Microbiol.* **4**, 2285–2297 (2019).
26. Reynolds, L. A. & Finlay, B. B. Early life factors that affect allergy development. *Nat. Rev. Immunol.* **17**, 518–528 (2017).
27. Gensollen, T., Iyer, S. S., Kasper, D. L. & Blumberg, R. S. How colonization by microbiota in early life shapes the immune system. *Science* **352**, 539–544 (2016).
28. Bokulich, N. A. et al. Antibiotics, birth mode, and diet shape microbiome maturation during early life. *Sci. Transl. Med.* **8**, 343ra82 (2016).
29. Shao, Y. et al. Stunted microbiota and opportunistic pathogen colonization in caesarean-section birth. *Nature* **574**, 117–121 (2019).
30. Pasolli, E. et al. Extensive unexplored human microbiome diversity revealed by over 150,000 genomes from metagenomes spanning age, geography, and lifestyle. *Cell* **176**, 649–662 (2019).
31. The Integrative HMP (iHMP) Research Network Consortium. The Integrative Human Microbiome Project. *Nature* **569**, 641–648 (2019).
32. Nash, A. K. et al. The gut mycobiome of the Human Microbiome Project healthy cohort. *Microbiome* **5**, 153 (2017).
33. Limon, J. J., Skalski, J. H. & Underhill, D. M. Commensal fungi in health and disease. *Cell Host Microbe* **22**, 156–165 (2017).
34. Koskinen, K. et al. First insights into the diverse human archaeome: specific detection of Archaea in the gastrointestinal tract, lung, and nose and on skin. *MBio* **8**, 00824-17 (2017).
35. Durán, P. et al. Microbial interkingdom interactions in roots promote *Arabidopsis* survival. *Cell* **175**, 973–983 (2018).
36. Carr, A., Diener, C., Baliga, N. S. & Gibbons, S. M. Use and abuse of correlation analyses in microbial ecology. *ISME J.* **13**, 2647–2655 (2019).
37. Contijoch, E. J. et al. Gut microbiota density influences host physiology and is shaped by host and microbial factors. *eLife* **8**, e40553 (2019).
38. Vandeputte, D. et al. Quantitative microbiome profiling links gut community variation to microbial load. *Nature* **551**, 507–511 (2017).
39. Stämmler, F. et al. Adjusting microbiome profiles for differences in microbial load by spike-in bacteria. *Microbiome* **4**, 28 (2016).
40. Ishwaran, H. & Rao, J. S. Spike and slab variable selection: frequentist and Bayesian strategies. *Ann. Stat.* **33**, 730–773 (2005).
41. Gonze, D., Coyte, K. Z., Lahti, L. & Faust, K. Microbial communities as dynamical systems. *Curr. Opin. Microbiol.* **44**, 41–49 (2018).
42. Bucci, V. et al. MDSINE: Microbial Dynamical Systems INference Engine for microbiome time-series analyses. *Genome Biol.* **17**, 121 (2016).
43. Freilich, M. A., Wieters, E., Broitman, B. R., Marquet, P. A. & Navarrete, S. A. Species co-occurrence networks: can they reveal trophic and non-trophic interactions in ecological communities? *Ecology* **99**, 690–699 (2018).
44. Friedman, J. & Alm, E. J. Inferring correlation networks from genomic survey data. *PLOS Comput. Biol.* **8**, e1002687 (2012).
45. Faust, K. et al. Microbial co-occurrence relationships in the human microbiome. *PLOS Comput. Biol.* **8**, e1002606 (2012).
46. Watts, S. C., Ritchie, S. C., Inouye, M. & Holt, K. E. FastSpar: rapid and scalable correlation estimation for compositional data. *Bioinformatics* **35**, 1064–1066 (2019).
47. Stein, R. R. et al. Ecological modeling from time-series inference: insight into dynamics and stability of intestinal microbiota. *PLOS Comput. Biol.* **9**, e1003388 (2013).
48. Fisher, C. K. & Mehta, P. Identifying keystone species in the human gut microbiome from metagenomic timeseries using sparse linear regression. *PLoS ONE* **9**, e102451 (2014).
49. Pammi, M., Liang, R., Hicks, J., Mistretta, T. A. & Versalovic, J. Biofilm extracellular DNA enhances mixed species biofilms of *Staphylococcus epidermidis* and *Candida albicans*. *BMC Microbiol.* **13**, 257 (2013).

Reporting summary

Further information on research design is available in the Nature Research Reporting Summary linked to this paper.

Data availability

All Illumina raw sequencing reads, including cohort samples and validation samples, have been deposited at the European Nucleotide Archive (ENA) under study accession number PRJEB36435. Source data for all figures are included in the Supplementary Tables. The public rDNA databases SILVA (119 release; https://www.arb-silva.de/documentation/release-119/) and UNITE (2017-12-01 release; https://unite.ut.ee/repository.php) were used to annotate the operational taxonomic unit (OTU) table.

Code availability

Custom scripts for microbiome analyses and interaction inference are available at https://github.com/katcoyte/MK-SpikeSeq.

Acknowledgements We thank all of the infants and their families who participated in the study; J. Xavier, J. Ordovas-Montanes, O. Cunrath and members of the Rakoff-Nahoum laboratory for discussions; and L. Martin for assistance with sample collection. K.Z.C. is funded by a Sir Henry Wellcome Postdoctoral Research Fellowship (grant 201341/A/16/Z) and a University of Manchester Presidential Fellowship; R.S.G. is supported by grants 1R01AI153257-01 and 5R01AI139633-03; and S.R-N. is supported by a Career Award for Medical Scientists from the Burroughs Wellcome Fund, a Pew Biomedical Scholarship, a Basil O'Connor Starter Scholar Award from the March of Dimes, P30DK040561, K08AI130392-01 and a NIH Director's New Innovator Award DP2GM136652.

Author contributions C.R., K.Z.C. and S.R.-N. conceived the project. C.R., K.Z.C. and W.B. performed the experiments. C.R. and K.Z.C. performed the computational analysis. C.R.M. designed the prospective cohort of infants and performed sample collection and metadata collation. C.R., K.Z.C. and S.R.-N. wrote the manuscript with contributions from all other authors.

Competing interests C.R.M. receives grant funding from Mead Johnson Nutrition. C.R.M. also provides consulting services for Mead Johnson Nutrition, Alcresta and Fresenius Kabi, and sits on the Scientific Advisory Boards of Plakous Therapeutics and LUCA Biologics. All other authors declare no competing interests.

Additional information

Supplementary information The online version contains supplementary material available at https://doi.org/10.1038/s41586-021-03241-8.

Correspondence and requests for materials should be addressed to K.Z.C. or S.R.-N.

Peer review information *Nature* thanks Jeff Gore and the other, anonymous, reviewer(s) for their contribution to the peer review of this work. Peer reviewer reports are available.

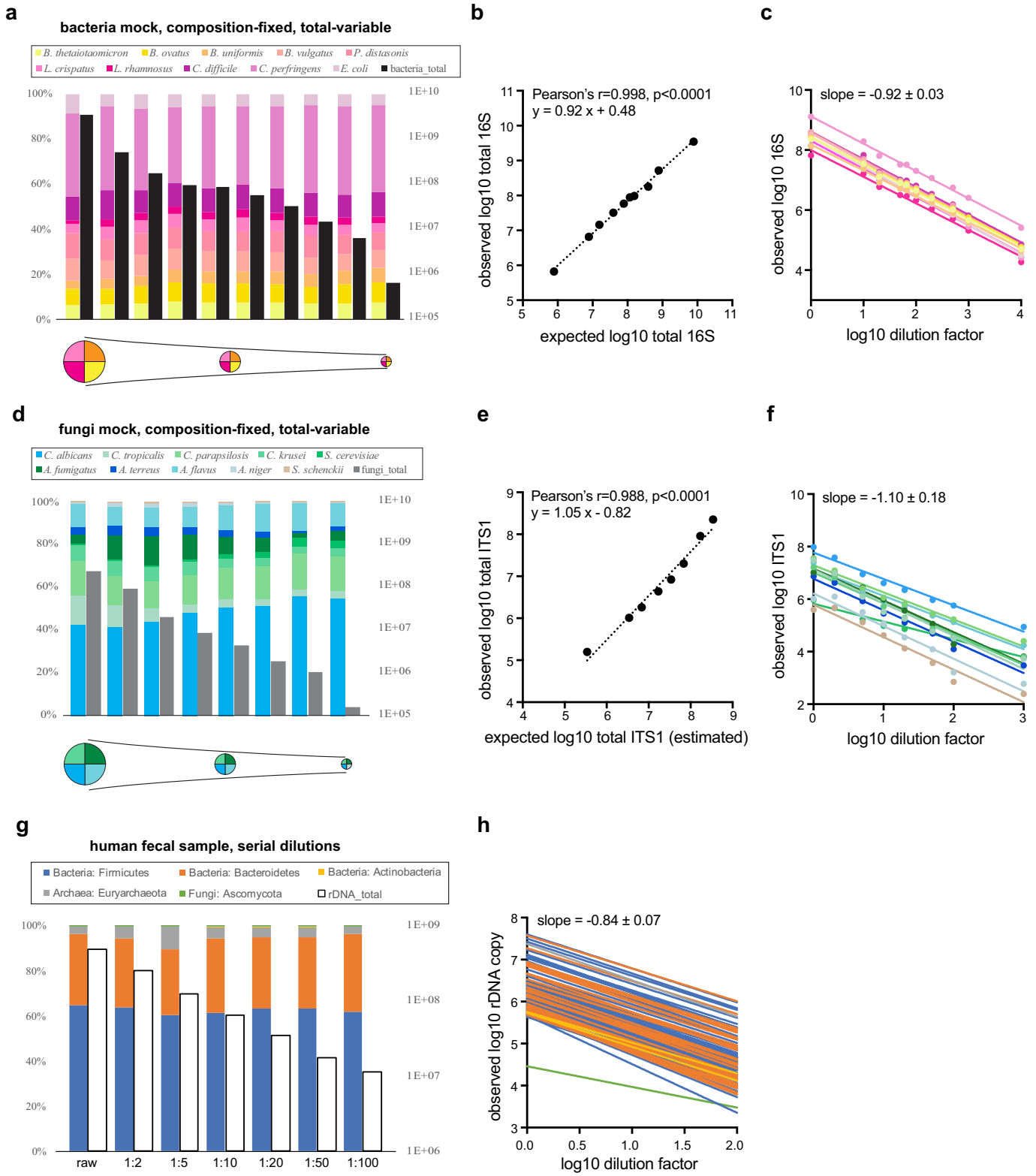

Extended Data Fig. 1 | MK-SpikeSeq reliably measures absolute abundances across kingdoms. a, **d**, A set of single-kingdom mock communities with a fixed composition of 10 bacterial (**a**) or 10 fungal (**d**) species and variable total microbial loads (indicated by the pie chart schematics underneath), were quantified using MK-SpikeSeq for relative composition (coloured bars) and absolute abundance (black or grey bars). **b**, **e**, Correlations between expected (based on initial microbial densities and known dilution factors) and MK-SpikeSeq-measured total absolute abundances of bacteria (**b**) and fungi (**e**) show that MK-SpikeSeq reliably detects absolute abundances of bacteria and fungi. For **e**, as exact rDNA copy numbers per fungal cell are undefined, the expected total abundances of internal transcribed spacer 1 (ITS1) are only estimates (here using 200 rDNA copies per fungal cell). **c**, **f**, Changes in absolute abundance for individual members (colour-coded as in **a**, **d**) of the bacterial (**c**) and fungal (**f**) mock communities are largely consistent with known dilution factors. **g**, A set of serial dilutions of a human faecal sample was quantified using MK-SpikeSeq for relative composition (coloured bars; shown are the phylum-level taxa) and absolute abundance (empty bars). **h**, Changes in absolute abundance for individual taxa (colour-coded in phyla as in **g**) across kingdoms are largely consistent with known dilution factors.

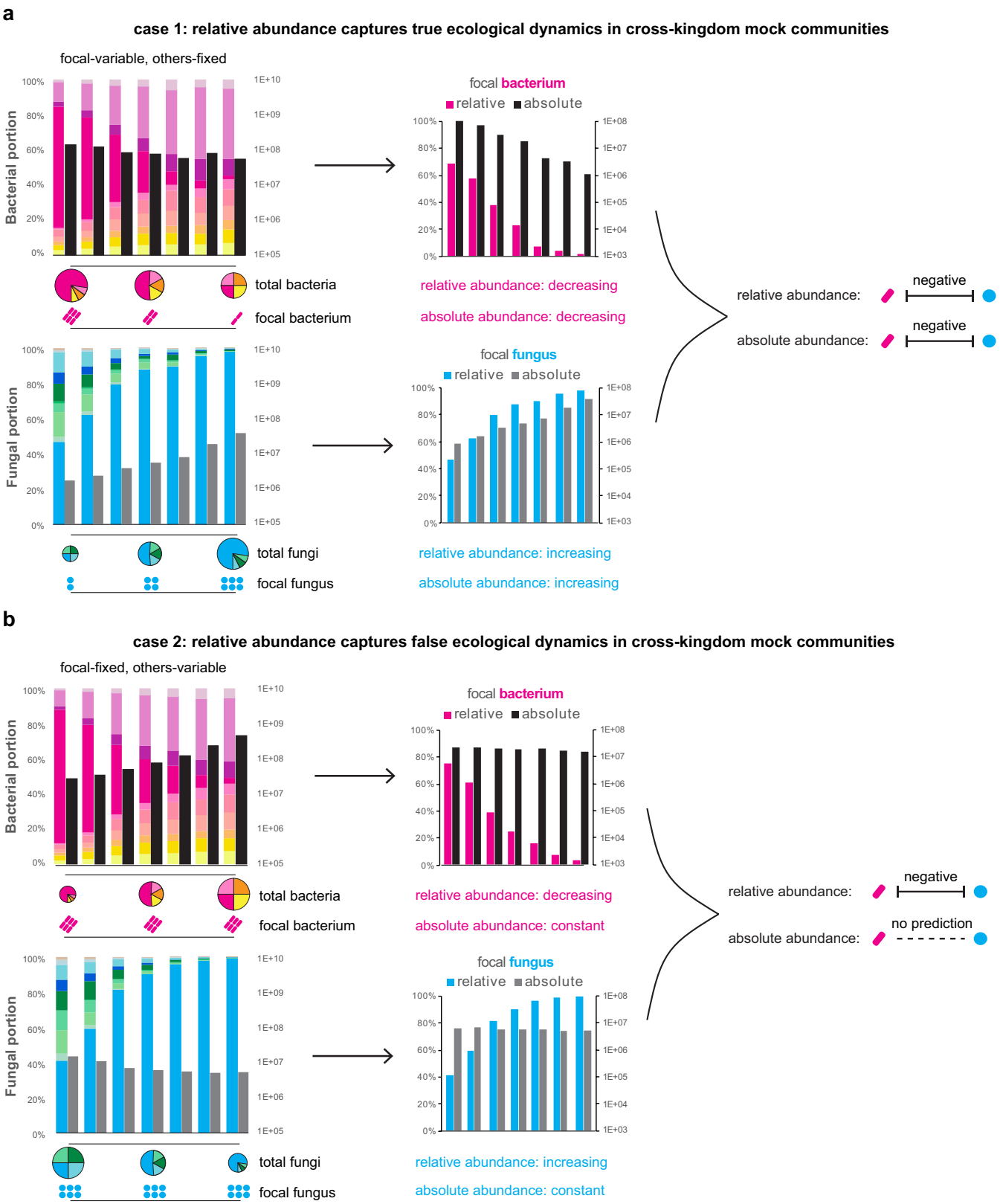

Extended Data Fig. 2 | MK-SpikeSeq captures key ecological dynamics in multi-kingdom mock communities. a, **b**, Two sets of defined multi-kingdom consortia, including ten bacteria and ten fungi (left, colour-coded as in Extended Data Fig. 1a, d), were assembled to model a 'true' (**a**) and a 'false' (**b**) negative interaction between one focal bacterium and one focal fungus, by varying the abundances of either these focal species or other background members. The MK-SpikeSeq quantifications of focal species highlight either consistent (**a**) or distinct (**b**) patterns between relative abundance and absolute abundance (middle). Relative abundance data may lead to a false prediction of cross-kingdom interaction between the focal species, whereas absolute abundance data measured by MK-SpikeSeq could disentangle these distinct mock ecological dynamics (right).

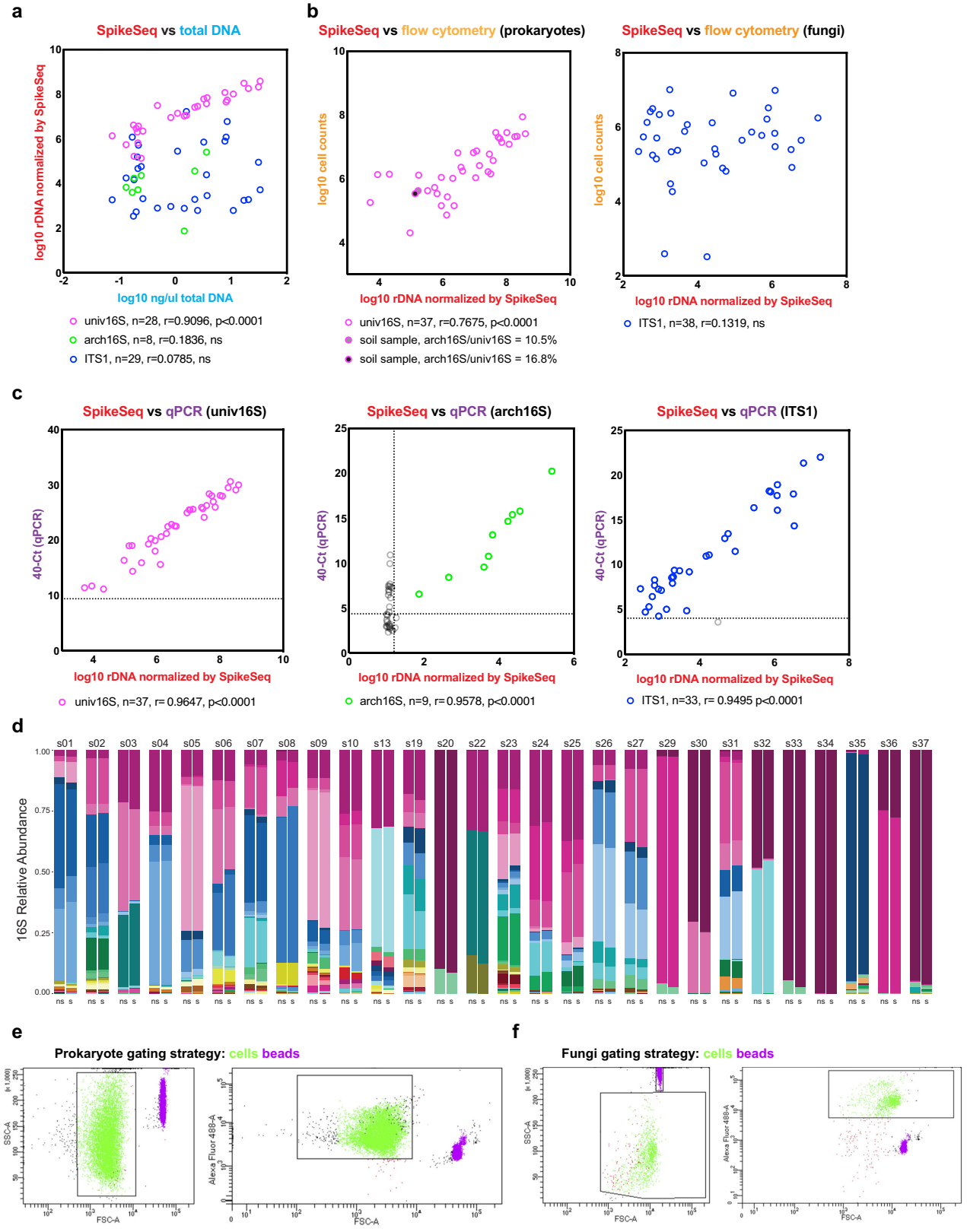

Extended Data Fig. 3 | See next page for caption.

Extended Data Fig. 3 | MK-SpikeSeq outperforms other quantification methods in cross-kingdom specificity. A set of 40 test samples including human stools and soil samples were used to compare kingdom-specific quantifications of absolute abundance. **a**, MK-SpikeSeq compared with total DNA yields. Pearson correlation tests show that total DNA yields mostly only reflect bacterial community abundances. **b**, MK-SpikeSeq compared with flow cytometry cell enumerations using gating strategies targeted for either prokaryotes or fungi. For prokaryotic enumerations, two soil samples are highlighted owing to their high archaeal loads that cannot be distinguished from bacterial counts by flow cytometry. For fungi enumerations, results using one gating strategy are shown; attempts using two additional gating strategies show a similar overestimation of fungal counts (Supplementary Table 4). **c**, MK-SpikeSeq compared with kingdom-specific qPCR. Horizontal dashed lines show the limit of detection using qPCR, based on the negative control (DNA extraction of water); vertical dashed line shows the limit of detection using MK-SpikeSeq, based on a minimum of one read of non-spike-in archaeal 16S (arch16S) normalized against the average arch16S sequencing depth. Samples below the limit of detection are excluded from correlational tests. Some samples with an arch16S signal lower than the MK-SpikeSeq limit of detection showed arch16S qPCR signals that were higher than the negative control, probably owing to bacterial signals bleeding into archaea-specific qPCR. For **a**–**c**, Pearson correlation *r* and two-sided *P* values are shown (no adjustment for multiple comparisons). **d**, Comparison of 16S genus-level profiles sequenced with (s) or without (ns) spike-in shows largely unaltered community compositions having exogenous spike-in. **e**, **f**, Flow cytometry gating strategies used in prokaryotic (**e**) and fungal (**f**) cell counting (see **b**), with green showing bacterial and fungal cells and purple showing microsphere particles provided in the bacteria-counting kit. Higher voltage settings were used in flow cytometry for prokaryote cell counting than for fungi cell counting.

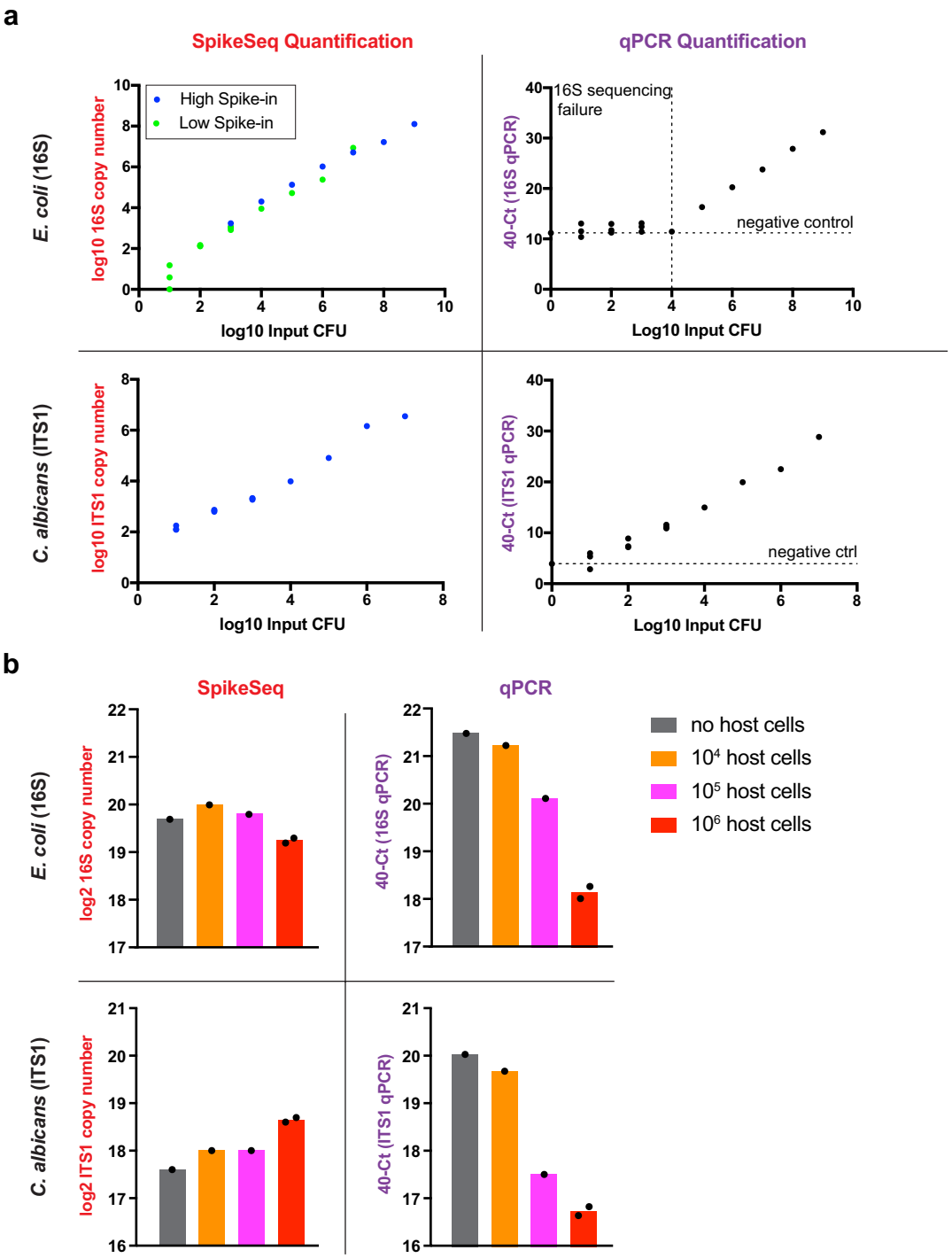

Extended Data Fig. 4 | MK-SpikeSeq outperforms qPCR in the sensitivity of detection and robustness to sample background. a, Comparison of sensitivity between MK-SpikeSeq and qPCR using tenfold serial dilutions of *Escherichia coli* and *C. albicans*. MK-SpikeSeq showed an increase in sensitivity of around 100–1,000-fold relative to qPCR in low-bacterial-abundance samples (detecting as few as 10 bacterial cells). For MK-SpikeSeq of *E. coli* samples, two levels of spike-in were used to cover the whole range of detection under the sequencing depth of around 10,000–100,000 reads per sample. For qPCR, horizontal dashed lines indicate the negative control (DNA extraction of water) and vertical dashed line shows the threshold below which pooled 16S sequencing yielded fewer than 100 reads (sequencing failed, probably owing to too low a signal). **b**, Comparison of robustness to host-cell background between MK-SpikeSeq and qPCR using test samples with fixed amounts of *E. coli* and *C. albicans* and a variable number of Caco-2 colonic cells. MK-SpikeSeq detected consistent (<2-fold variations) microbial abundances in samples with high host-cell background whereas qPCR under-measured microbial abundances by tenfold ($\Delta C_t > 3.3$). $n = 2$ for the 10^6 host cells group; $n = 1$ for the other groups.

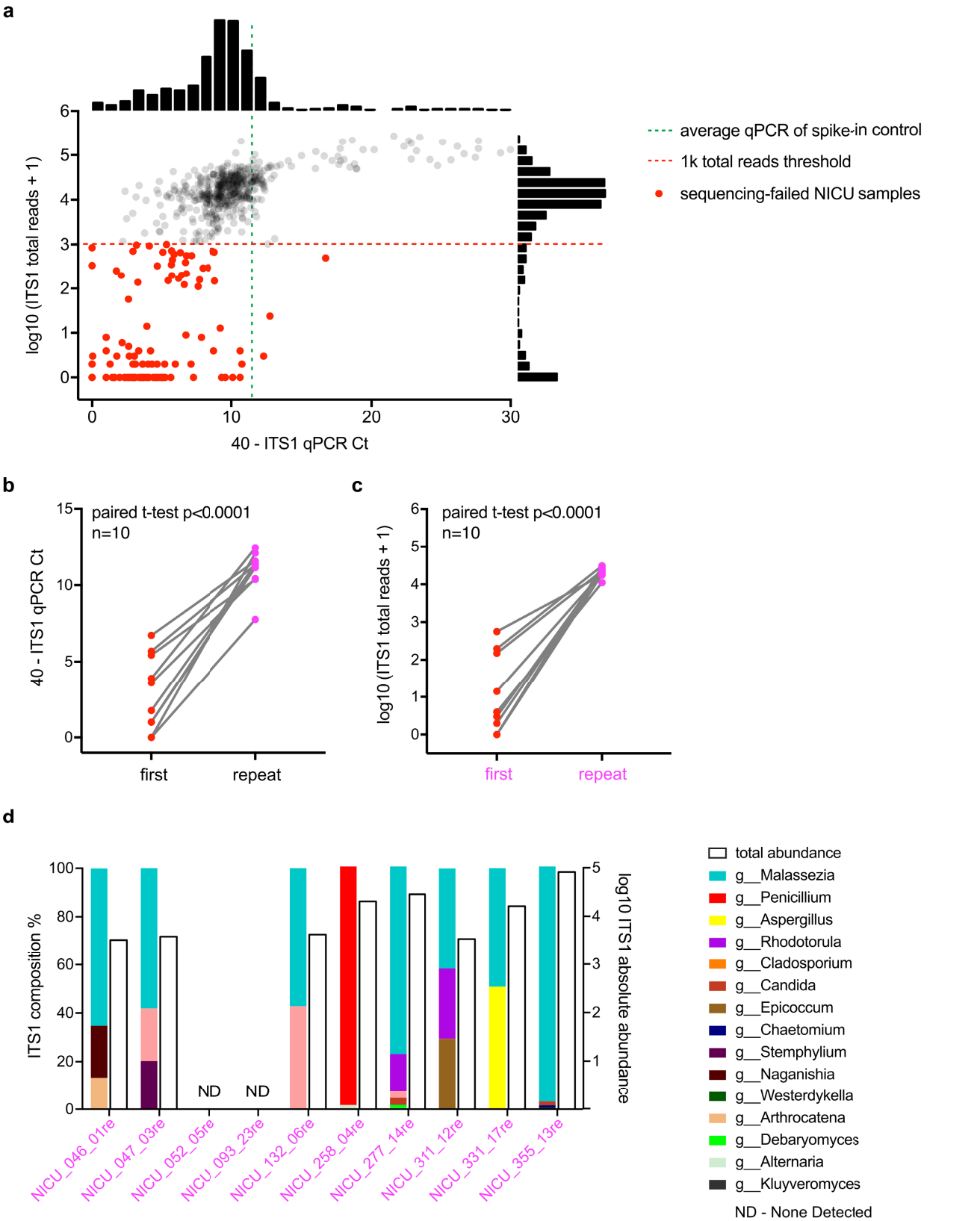

Extended Data Fig. 5 | MK-SpikeSeq identifies errors in sample processing of fungal communities. a, In our first phase of NICU sequencing (Supplementary Information), we identified a number of samples (highlighted in red dots) that failed to yield more than 1,000 ITS1 reads per sample after quality filtering (red dashed line). Many of these samples that failed sequencing showed much lower ($\Delta C_t > 5$) ITS1 qPCR signals than the spike-in control (green dashed line), indicating poor DNA extractions of fungi in these samples. Frequency histograms of measurements are shown next to the axes. **b**, Reprocessing of 10 of these samples that failed sequencing led to increased ITS1 qPCR signals, indicating improved DNA extractions. **c**, These reprocessed samples also yielded the desired number (over 10,000) of ITS1 reads, passing our rDNA-sequencing criteria. *P* values by two-tailed paired Student's *t*-test (**b**, **c**). **d**, Eight of the reprocessed samples showed non-zero fungal communities, and only two had no detectable fungal signal. The composition (coloured bars) and total abundance (empty bars) of fungal communities in these reprocessed samples are shown.

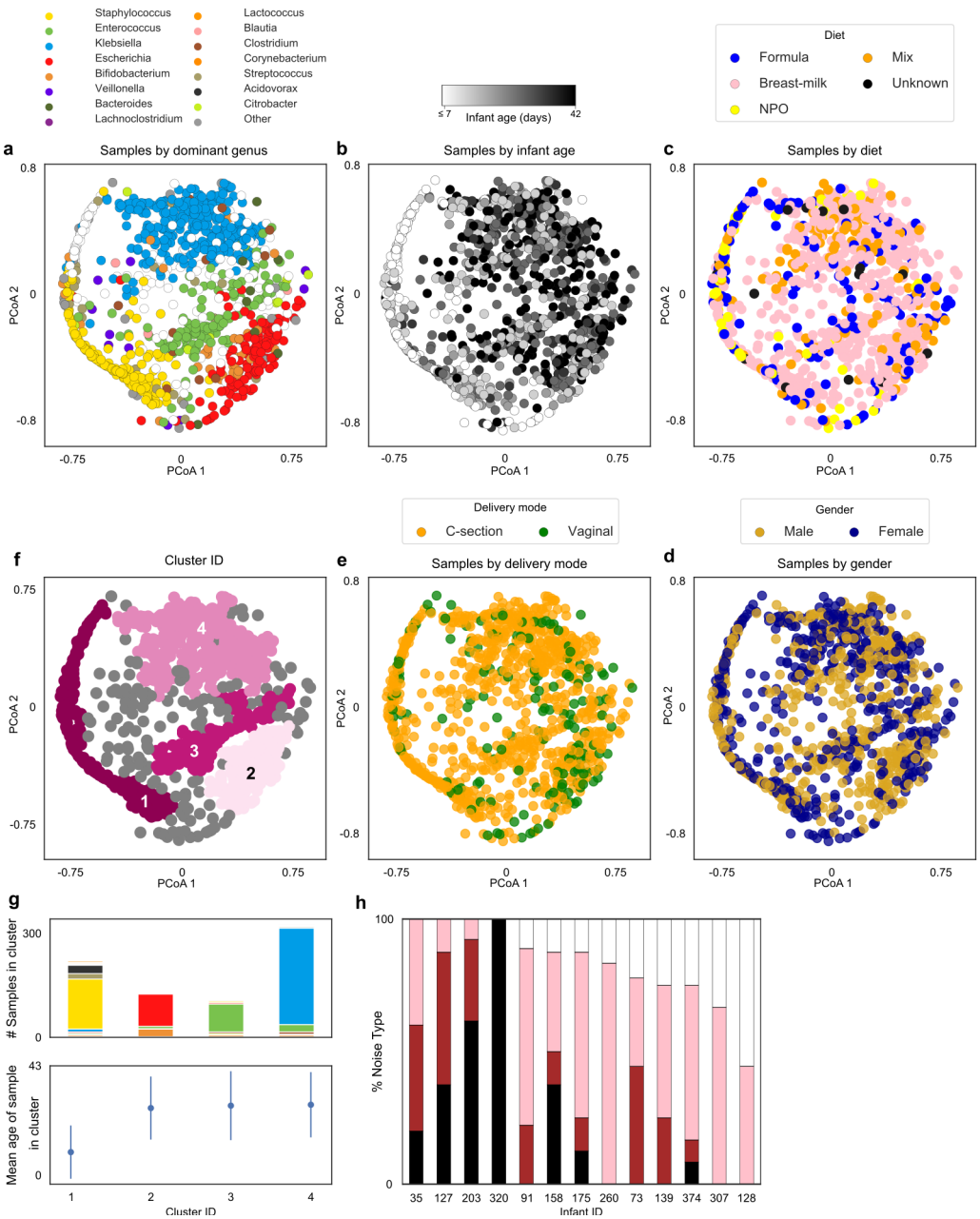

Extended Data Fig. 6 | Bacterial samples cluster according to composition and infant age, but not according to infant diet, delivery mode or sex. **a**, PCoA based on Bray–Curtis dissimilarities of bacterial community composition between samples (genus level). Samples are coloured by dominant taxa or are shown in white when diversity is high (IS > 4). **b**, PCoA with samples coloured by infant age. **c**, PCoA with samples coloured by infant diet. **d**, PCoA with samples coloured by the sex of the infant. **e**, PCoA with samples coloured by delivery mode. **f**, PCoA with samples coloured by cluster membership, calculated using DBSCAN (density-based spatial clustering of applications with noise). **g**, Stacked bars represent the distribution of the dominant genus within each cluster and dot plots illustrate the average day of life of samples within each cluster. A Kruskal–Wallis test with Bonferroni correction showed statistically significant differences in day of life of samples between clusters ($X^2 = 254$, $P << 0.0001$, degrees of freedom (df) = 3). Data are mean ± s.d. **h**, Stacked bars indicate the proportion of genera exhibiting each type of noise per infant. Dark noise indicates increasing temporal dependence; white noise suggests that temporal dynamics are entirely random.

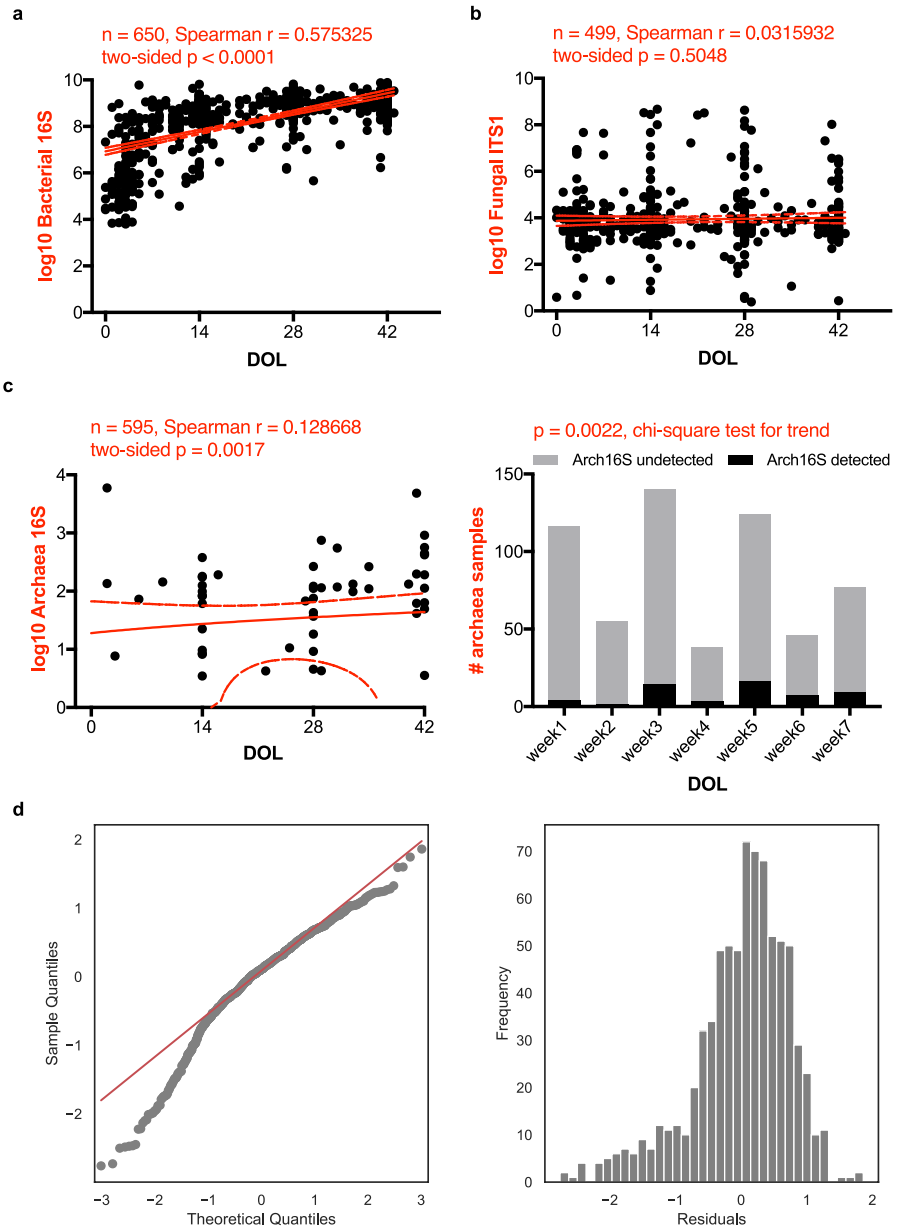

Extended Data Fig. 7 | Trends in total microbial loads for all three kingdoms. a–**c**, Scatter plots of rDNA-based total abundances of bacteria (**a**), fungi (**b**) and archaea (**c**) against infant day of life (DOL), measured by MK-SpikeSeq in the first phase. The red lines denote the linear regression fit and the 90% confidence bands of the best-fit line of absolute abundances on a logarithmic scale. Spearman correlations show that bacterial and archaeal—but not fungal—loads are positively associated with infant age. Samples with an undetectable kingdom-specific rDNA signal are not plotted. For archaea that show scarce signal in the cohort (**c**, left), a separate presence–absence plot and X^2 test of binned samples (**c**, right) also show a positive correlation between archaeal loads and infant age. **d**, Diagnostics for linear mixed-effects model.

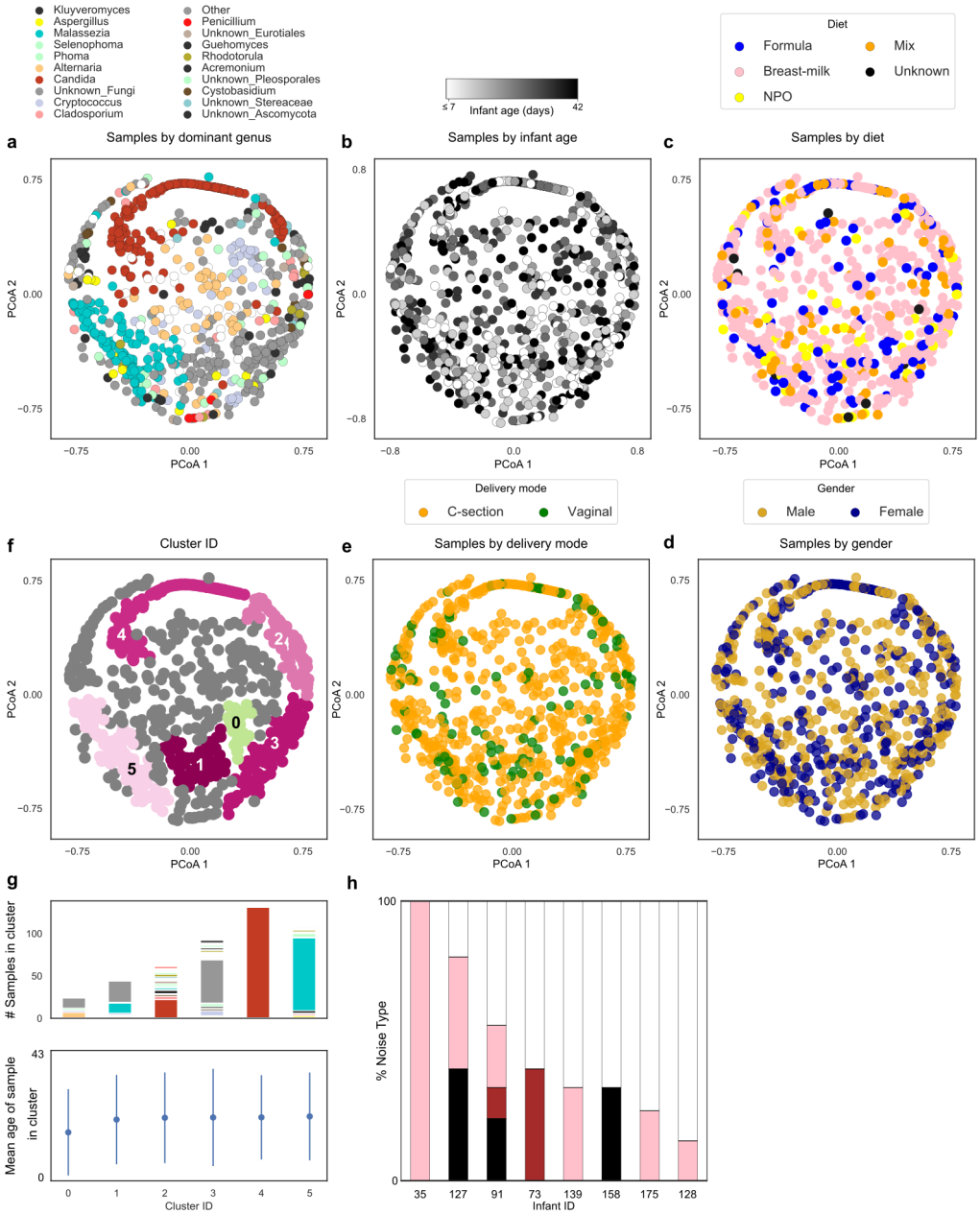

Extended Data Fig. 8 | Fungal community composition does not map to infant age, diet, sex or delivery mode. a, PCoA based on Bray–Curtis dissimilarities of fungal community composition between samples (genus level). Samples are coloured by dominant taxa or are shown in white when diversity is high (IS > 4). **b**, PCoA with samples coloured by infant age. **c**, PCoA with samples coloured by infant diet. **d**, PCoA with samples coloured by the sex of the infant. **e**, PCoA with samples coloured by delivery mode. **f**, PCoA with samples coloured by cluster membership, calculated using the DBSCAN algorithm. **g**, Stacked bars represent the distribution of the dominant genus within each cluster and dot plots illustrate the average day of life of samples within each cluster. A Kruskal–Wallis test with Bonferroni correction showed no statistically significant differences in day of life of samples between clusters ($X^2 = 3.06$, $P = 0.69$, df = 5). Data are mean ± s.d. **h**, Stacked bars indicate the proportion of genera exhibiting each type of noise per infant. Dark noise indicates increasing temporal dependence; white noise suggests that temporal dynamics are entirely random. Notably, the mycobiomes of five infants could not be classified.

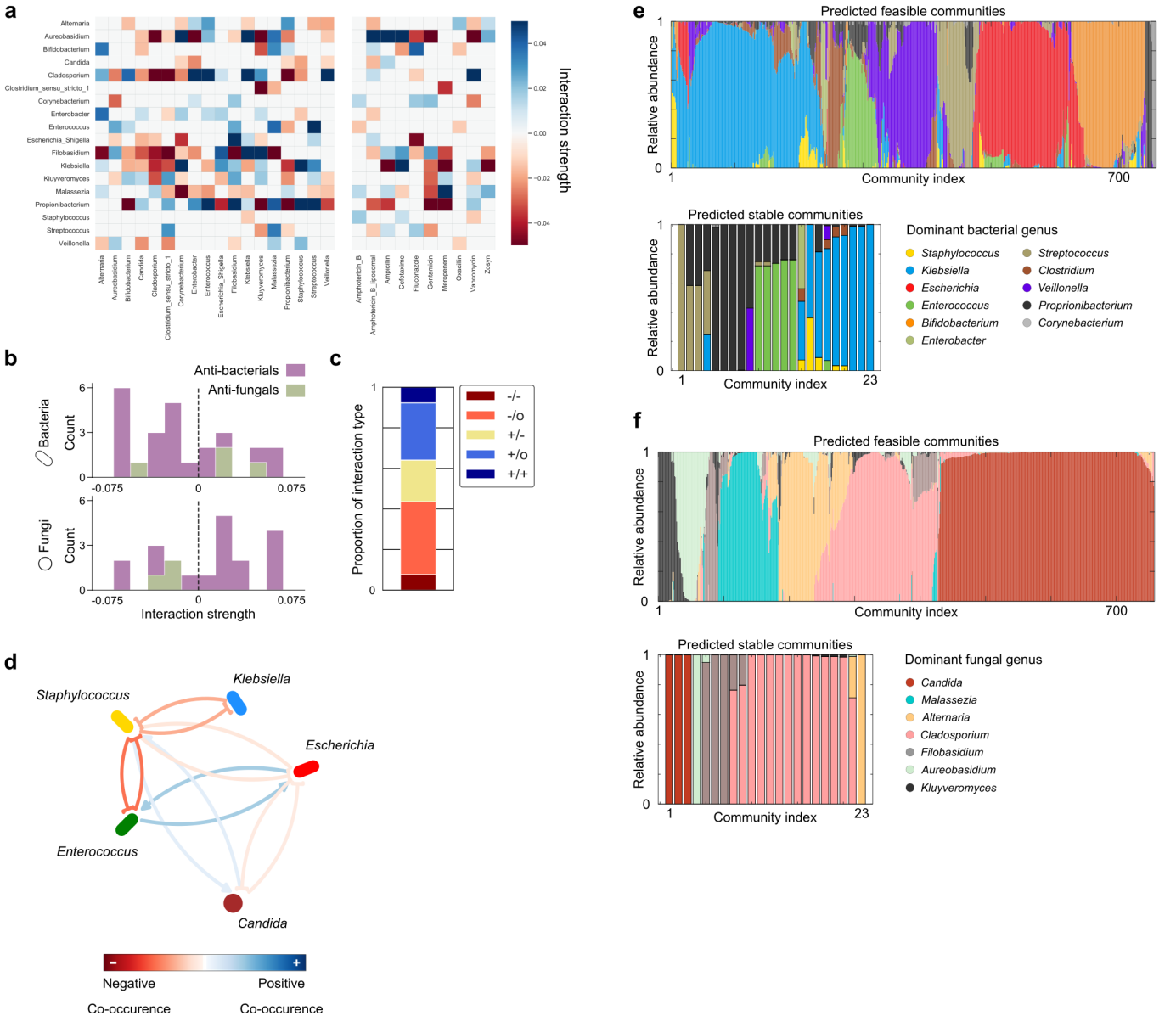

Extended Data Fig. 9 | Microbe–microbe interactions are predominantly asymmetric, and inferring interactions from data that are based on relative abundance generates misleading results. a, Heat map plotting interactions inferred by the gLV model. Each row of the heat map illustrates the effect on the target genera by other members of the gut community (left columns) or documented use of antimicrobial agents according to the clinical metadata (right columns). **b**, Histogram of individual antibacterial (purple) or antifungal (green) interaction strengths, split by kingdom. Antibacterial agents primarily inhibit bacteria, and antifungal agents primarily inhibit fungi; however, there is not a significant bias in the likelihood of either antimicrobial agent inhibiting their target kingdom (exact binomial tests, null hypothesis H0: $P(\text{Inhibition}) = 0.5, P > 0.05$). **c**, Stacked bar shows the proportion of different interaction types occurring between genera. Over 80% of interactions are asymmetric, being either exploitative (+/−), commensal (+/0) or amensal (−/0). **d**, To confirm the value of our absolute abundance methods, we inferred inter-genus interactions from relative abundance data alone using the FastSpar[46] algorithm. This approach robustly identifies co-occurrence relationships between different microbial taxa in a manner that accounts for the compositional nature of relative abundance data. Notably, correlation networks cannot infer asymmetric interactions, thus this approach cannot detect the exploitation of *Staphylococcus* by *Klebsiella*. It also erroneously infers that *Staphylococcus* increases the growth of *Candida*, and cannot detect the inhibition of *Klebsiella* by *Candida* or *Enterococcus*. **e**, Steady-state relative abundances of bacteria of those subcommunities predicted to be feasible and/or linearly asymptotically stable. **f**, Steady-state relative abundances of fungi of those subcommunities predicted to be feasible and/or linearly asymptotically stable.

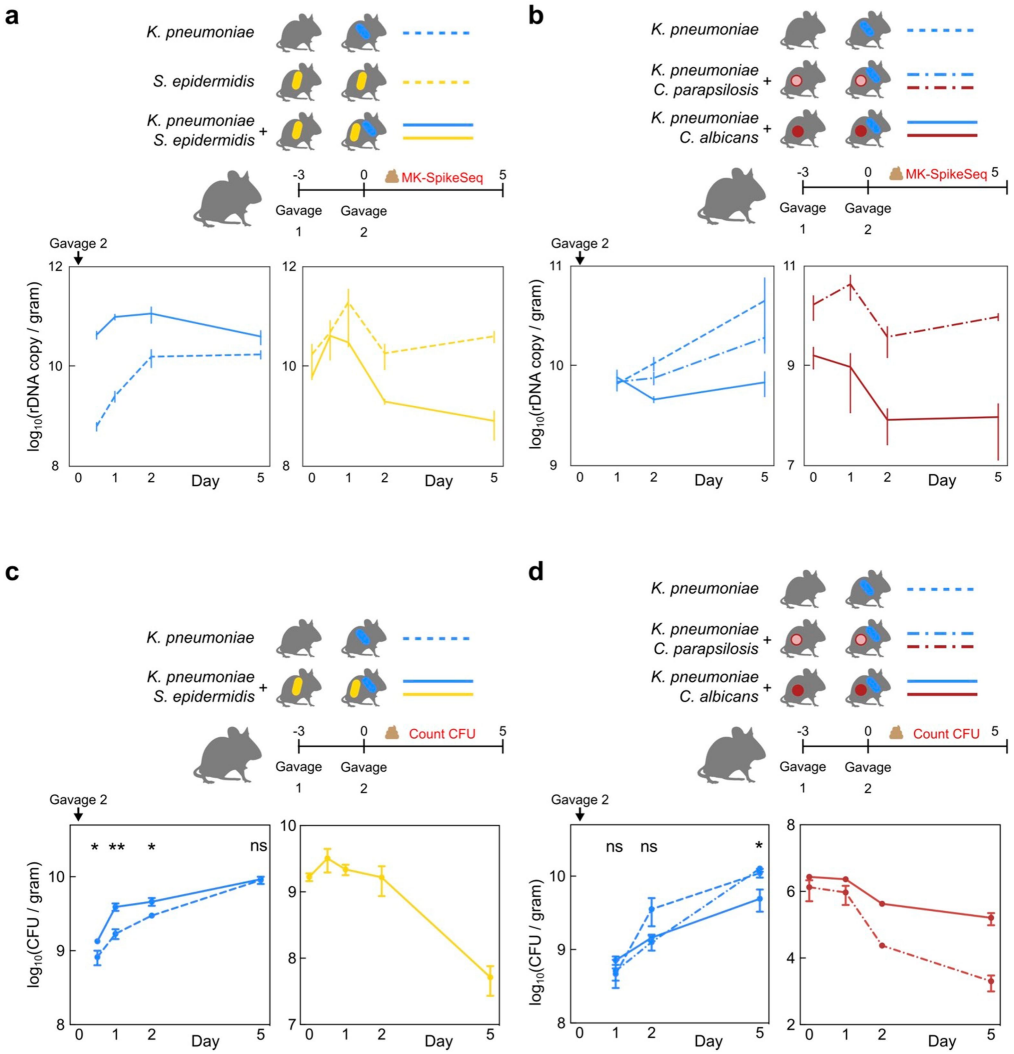

Extended Data Fig. 10 | MK-SpikeSeq measurement and repeat experiments of in vivo colonization. a, **b**, Biological replicate samples of mouse stools characterized by CFU counting of strains of interest in Fig. 3d, f were subjected to MK-SpikeSeq to determine rDNA-based absolute abundances of the specified strains (**a**, MK-SpikeSeq measurement for Fig. 3d; **b**, MK-SpikeSeq measurement for Fig. 3f). **c**, **d**, Repeat in vivo colonization experiments (**c**, repeat of Fig. 3d; **d**, repeat of Fig. 3f). Data are mean ± s.e.m.; $^{*}P < 0.05$, $^{**}P < 0.01$ (by two-tailed Student's *t*-test). For **c**, $n = 5$ per group, *t*-test of *K. pneumoniae* CFU between the groups with or without *S. epidermidis* pre-colonization. For **d**, $n = 4$ for the *C. albicans* + *K. pneumoniae* group, $n = 3$ for the other two groups, *t*-test of *K. pneumoniae* CFU between *C. albicans* and *C. parapsilosis* groups. See Supplementary Table 15 for exact *P* values.

nature research

Corresponding author(s): Seth Rakoff-Nahoum

Last updated by author(s): Nov 16, 2020

Reporting Summary

Nature Research wishes to improve the reproducibility of the work that we publish. This form provides structure for consistency and transparency in reporting. For further information on Nature Research policies, see Authors & Referees and the Editorial Policy Checklist .

Statistics

For all statistical analyses, confirm that the following items are present in the figure legend, table legend, main text, or Methods section.

n/a	Confirmed
☐	☒ The exact sample size (*n*) for each experimental group/condition, given as a discrete number and unit of measurement
☐	☒ A statement on whether measurements were taken from distinct samples or whether the same sample was measured repeatedly
☐	☒ The statistical test(s) used AND whether they are one- or two-sided *Only common tests should be described solely by name; describe more complex techniques in the Methods section.*
☐	☒ A description of all covariates tested
☐	☒ A description of any assumptions or corrections, such as tests of normality and adjustment for multiple comparisons
☐	☒ A full description of the statistical parameters including central tendency (e.g. means) or other basic estimates (e.g. regression coefficient) AND variation (e.g. standard deviation) or associated estimates of uncertainty (e.g. confidence intervals)
☐	☒ For null hypothesis testing, the test statistic (e.g. *F*, *t*, *r*) with confidence intervals, effect sizes, degrees of freedom and *P* value noted *Give P values as exact values whenever suitable.*
☐	☒ For Bayesian analysis, information on the choice of priors and Markov chain Monte Carlo settings
☒	☐ For hierarchical and complex designs, identification of the appropriate level for tests and full reporting of outcomes
☐	☒ Estimates of effect sizes (e.g. Cohen's *d*, Pearson's *r*), indicating how they were calculated

Our web collection on statistics for biologists contains articles on many of the points above.

Software and code

Policy information about availability of computer code

Data collection	None
Data analysis	Amplicon sequencing reads were analysed using custom R (v3.0.1) and Python (v2.7 & 3.7) code that is freely available on our github repository (https://github.com/katcoyte/MK-SpikeSeq). Flow cytometry data were analyzed using BD FACSDiva software (v. 8.0.1). Statistics of Pearson correlation and Student's t test were performed in GraphPad Prism (v7.0a). Dimensionality reduction and clustering were performed using DBSCAN and MDS functions from sklearn (version 0.22.1). Correlation analyses were performed using the FastSpar algorithm (https://doi.org/10.1093/bioinformatics/bty734). Noise analyses were performed using the R package 'seqtime' version 0.1.1 (https://github.com/hallucigenia-sparsa/seqtime).

For manuscripts utilizing custom algorithms or software that are central to the research but not yet described in published literature, software must be made available to editors/reviewers. We strongly encourage code deposition in a community repository (e.g. GitHub). See the Nature Research guidelines for submitting code & software for further information.

Data

Policy information about availability of data

All manuscripts must include a data availability statement. This statement should provide the following information, where applicable:

- Accession codes, unique identifiers, or web links for publicly available datasets
- A list of figures that have associated raw data
- A description of any restrictions on data availability

All non-clinical data associated with the study are available on our github repository (https://github.com/katcoyte/MK-SpikeSeq). De-identified clincal metadata are available on request. All Illumina sequencing raw read, including cohort samples and validation samples, have been deposited at the European Nucleotide Archive (ENA) under study accession no. PRJEB36435. Source data for all figures are included in Supplemental Tables (Table 3 - ED Fig 1/2; Table 4 - ED Fig 3; Table 5 - ED Fig 4; Table 6 - ED Fig 5; Table 8~10 - Fig2, ED Fig 6~8; Table 11~12 - Fig 2; Table 14 - Fig 3c/e; Table 15 - Fig 3d/f, ED Fig 10). Public rDNA databases SILVA (119 release, www.arb-silva.de/documentation/release-119/) and UNITE (2017-12-01 release, unite.ut.ee/repository.php) were used to annotate OTU tables.

Field-specific reporting

Please select the one below that is the best fit for your research. If you are not sure, read the appropriate sections before making your selection.

☒ Life sciences ☐ Behavioural & social sciences ☐ Ecological, evolutionary & environmental sciences

For a reference copy of the document with all sections, see nature.com/documents/nr-reporting-summary-flat.pdf

Life sciences study design

All studies must disclose on these points even when the disclosure is negative.

Sample size	For the NICU cohort, no sample size calculation was conducted as we were not testing for end clinical outcomes nor testing any intervention. Sample sizes therefore represent the maximum number of samples possible given fiscal limitations and are sufficiently broad for a descriptive study. For animal studies, samples sizes were chosen to ensure statistical power.
Data exclusions	A fraction of NICU rDNA amplicon samples were excluded from OTU tables due to amplicon sequencing not achieving the required depth (> 1K total read counts and > 10 spike-in counts), dropping 3 bacterial, 56 archaeal and 152 fungal samples in the NICU Nextseq data, and 28 fungal samples in the NICU Miseq data.
Replication	All in vitro interaction pairs (Fig 3c/e) were replicated with 4-24 unique strain combinations, each with at least one biological replicate. All in vivo experiments contained 3-5 biological replicates (mice) per group, with experiments repeated to ensure against cage effects (8-10 biological replicates per treatment total, Fig 3d/f, Extended Data Figure 10c/d).
Randomization	No random allocation was used in the NICU cohort as our study was observational and thus did not test any intervention or grouping. For animal studies, mice were randomized into separate cages upon arrival from Jackson Laboratory.
Blinding	No blinding was used in the NICU cohort study as our study was observational and did not test any intervention or grouping. Illumina sequencings were not blinded due to the requirement of clear sample labelling. Blinded CFU counting was used in the in vitro and in vivo experiments (Fig 3, Extended Data Figure 10c/d).

Reporting for specific materials, systems and methods

We require information from authors about some types of materials, experimental systems and methods used in many studies. Here, indicate whether each material, system or method listed is relevant to your study. If you are not sure if a list item applies to your research, read the appropriate section before selecting a response.

Materials & experimental systems

n/a	Involved in the study
☒	☐ Antibodies
☒	☐ Eukaryotic cell lines
☒	☐ Palaeontology
☐	☒ Animals and other organisms
☐	☒ Human research participants
☒	☐ Clinical data

Methods

n/a	Involved in the study
☒	☐ ChIP-seq
☐	☒ Flow cytometry
☒	☐ MRI-based neuroimaging

Animals and other organisms

Policy information about studies involving animals; ARRIVE guidelines recommended for reporting animal research

Laboratory animals	C57BL/6J specific pathogen free 6~8 weeks old female mice (Jackson Laboratory, Bar Harbor, Maine), housed under 21.7 °C, 35%-65% humidity and 12:12 light/dark cycle.
Wild animals	No wild animals involved
Field-collected samples	No field samples collected
Ethics oversight	C57BL/6J SPF mice; animal protocol 18-02-3637R approved by the Institutional Animal Care and Use Committee at Boston Children's Hospital

Note that full information on the approval of the study protocol must also be provided in the manuscript.

Human research participants

Policy information about studies involving human research participants

Population characteristics	Discarded stool samples were collected from premature infants less than 33 weeks gestational age (approximately 50:50 male:female). Exclusion criteria for the biorepository included infants who died within 48 hours after birth, required transfer outside of the hospital immediately after birth, or were born to mothers with limited proficiency in English.
Recruitment	Preterm infants were retrospectively selected from an ongoing biorepository cohort referred to as the Infant Health Research Pro-gram (IHRP) at Beth Israel Deaconess Medical Center (BIDMC) in Boston, Massachusetts. The IHRP was established to evaluate the impact of nutrition on health and disease and includes longitudinal discarded biological samples annotated with clinical data from preterm infants born less than 33 weeks of gestation. The institutional review board at BIDMC in Boston, Massachusetts, approved the collection of discarded specimens from infants in the neonatal intensive care unit for the IHRP and the analyses performed in this study. All data was de-identified for use in this study. Verbal consent was obtained from the infant's parents when in the NICU (IRB protocol number 2009P-000014).
Ethics oversight	Beth Israel Deaconess Medical Center Institutional Review Board approved the study (protocol 2017P-000632)

Note that full information on the approval of the study protocol must also be provided in the manuscript.

Flow Cytometry

Plots

Confirm that:

☒ The axis labels state the marker and fluorochrome used (e.g. CD4-FITC).

☒ The axis scales are clearly visible. Include numbers along axes only for bottom left plot of group (a 'group' is an analysis of identical markers).

☒ All plots are contour plots with outliers or pseudocolor plots.

☒ A numerical value for number of cells or percentage (with statistics) is provided.

Methodology

Sample preparation	We diluted samples further by 10 fold in 2% paraformaldehyde. We used the Bacteria Counting Kit (Invitrogen, Cat B7277) for cell staining.
Instrument	We did flow cytometry on a LSRFortessa 3-laser cell analyzer (BD Biosciences, San Jose, CA).
Software	We used BD FACSDiva software (v. 8.0.1) for cell enumeration.
Cell population abundance	We calculated the cell abundances according to the normalization instruction in the Bacteria Counting Kit.
Gating strategy	We applied different flow settings and FSC/SSC/Alexa-Fluor-488 gating strategies for prokaryotes and fungi, pre-determined using axenic bacterial (E. coli) and fungal (C. albicans) cultures as positive controls (see Extended Data Fig 3e, f for example gating strategies). While prokaryotic gating was relatively robust against background noise, we found it was difficult to identify a gating specific for fungi against background (e.g., food debris and host cells). As a result, fungal cell counts were consistently over-estimated using three different gating strategies (see Supplemental Table 3).

☒ Tick this box to confirm that a figure exemplifying the gating strategy is provided in the Supplementary Information.